CROATICA CHEMICA ACTA
CCACAA, ISSN 0011-1643, e-ISSN 1334-417X
Croat. Chem. Acta **87** (4) (2014) 413–422.
http://dx.doi.org/10.5562/cca2489

Original Scientific Article

Analysis of the E–E Bond in Group-13 Complexes $[(PMe_3)_2(E_2H_n)]$ (E = B – In, n = 4, 2, 0)†

Nicole Holzmann* and Gernot Frenking*

Fachbereich Chemie, Philipps-Universität Marburg, Hans-Meerwein-Strasse, D-35032 Marburg, Germany

RECEIVED JUNE 3, 2014; REVISED AUGUST 13; 2014; ACCEPTED AUGUST 27, 2014

Abstract. Quantum chemical calculations at the BP86/def2-TZVPP level have been carried out for the donor-acceptor complexes $[(PMe_3)_2(E_2H_n)]$ for n = 4, 2, 0. The focus of this works lies on the E–E bonding situation. The electronic structure of the molecules was analyzed with the EDA-NOCV method and with NBO calculations. The EDA-NOCV analysis of the E–E interactions in $[(PMe_3)_2(E_2H_n)]$ (n = 4, 2, 0) provide deep insights into the nature and the strength of the bonds. The calculated intrinsic interactions ΔE_{int} suggest that the trend for the bond strength of the E–E single bond $[(PMe_3)(H)_2E–E(H)_2(PMe_3)]$ has the order B > Ga > Al > In. The orbital interactions ΔE_{orb} which exhibit the same trend as ΔE_{int} have one dominant contribution which comes from the coupling of the singly occupied orbitals in the $(PMe_3)(H)_2E$ fragments. A slightly different trend B > Ga ~ In > Al is found for the interaction energy ΔE_{int} of the E–E bonds in $[(PMe_3)(H)E–E(H)(PMe_3)]$. The orbital term ΔE_{orb} which has the order B > Ga > In > Al has one major and one minor component which in case of the boron compound may be identified with a σ and a π bond. The heavier homologues $[(PMe_3)(H)E–E(H)(PMe_3)]$ (E = Al–In) have pyramidally coordinated atoms E. The dominant orbital interactions in the latter species come from the formation of a "slipped" π bond while the minor component comes from the formation of the σ bond. This can be explained with the change in the hybridization of the orbitals at atom E along the formation of the E–E bond. The compounds $[(PMe_3)E–E(PMe_3)]$ exhibit three different types of bonding situations depending on atoms E. The boron system $[(PMe_3)B≡B(PMe_3)]$ has a classical triple bond which consist of a σ bond that provides 56 % to the orbital interactions and two degenerate π bonds which contribute 40 % to the covalent bonding. The aluminium and gallium complexes $[(PMe_3)E–E(PMe_3)]$ (E = Al, Ga) are also triply bonded species where the covalent bonding has one strong and two weaker components. The strong component comes from the "slipped" π bond while the minor components come from the formation of the σ and π bonds. The indium complex $[(PMe_3)In–In(PMe_3)]$ has only an In–In single bond and two electron lone pairs at the indium atoms. The charge donation $Me_3P \rightarrow E_2(H_n) \leftarrow PMe_3$ has for all atoms E the trend for n 4 > 2 > 0.

Keywords: donor-acceptor complex, bond multiplicity, bonding analysis, EDA-NOCV, quantum chemical calculations

INTRODUCTION

Recently, we reported a structure and bonding analysis of the donor-acceptor bonds in the group-13 complexes $[(L)_2(E_2H_n)]$ with n = 4, 2, 0 and ligand L being an N-heterocyclic carbene (NHC) or a phosphine ligand PMe_3.[1,2] Substituted derivatives of low-valent and low oxidation state hydrides such as $[(NHC^{Dipp})_2(B_2H_4)]$,[3] $[(NHC^{Dipp})_2(Al_2H_4)]$,[4] $[(NHC^{Dipp})_2(B_2H_2)]$[5] or $[(PPh_3)_2(B_2H_4)]$[6] are experimentally known. Lately, the complex $[(NHC^{Dipp})_2(B_2)]$ which is the first group-13 dimer E_2 stabilized in a complex $L \rightarrow E_2 \leftarrow L$ was isolated[7] which has a B≡B triple bond.[8] The calculations showed that the structural motives of the complexes $[(L)_2(E_2H_n)]$ differ significantly with the nature of the ligand L and the group-13 atom E.[1,2] While all analyzed complexes $[(L_2)(E_2H_4)]$ adopt C_s symmetry with trans oriented ligands, the heteroatoms E in the $[(L_2)(E_2H_2)]$ compounds are planar coordinated only for the boron complexes and for the NHC ligated aluminum and gallium dimers. The remaining complexes $[(L_2)(E_2H_2)]$ show pyramidal coordination at atom E. For the complexes $[(L_2)(E_2)]$ three structure motives were found: The stabilized boron dimers show a linear L–B–B–L arrangement, the heavier NHC complexes and the aluminum and gallium PMe_3 dimers have antiperiplanar

† Dedicated to Dr. Mirjana Eckert-Maksić on the occasion of her 70th birthday.

* Authors to whom correspondence should be addressed. (E-mail: holzmann@staff.uni-marburg.de, frenking@chemie.uni-marburg.de)

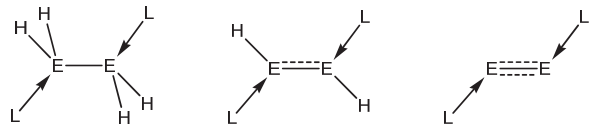

1E **2E** **3E**

Scheme 1. Schematic representation of the complexes $[(L)_2(E_2H_n)]$ with L = NHC^{Me}, PMe_3 and n = 4, 2 and 0. Dashed lines indicate different possible bonding modes.

coordinated ligands while in $[(PMe_3)_2(In_2)]$ the phosphine ligands are gauche oriented with an P–In–In–P dihedral angle of 123.0°.[1,2]

The theoretical findings pose the question about the nature of the E–E bonding in the complexes $[(L)_2(E_2H_n)]$ and the electronic state of the interacting fragments which could help to explain the different structures of the adducts (Scheme 1). In our previous studies we focused on the donor-acceptor interactions L → $E_2(H_n)$ ← L.[1,2] The nature of the E–E bonding was not discussed in this work. Therefore, we analyzed the nature of the E–E bonding with the EDA (Energy Decomposition Analysis) method in conjunction with the NOCV (Natural Orbitals for Chemical Valence) scheme.[9] Since the nature of the E–E bonding does not change when L = PR_3 or NHC, we restricted our work on the phosphine model compounds where L = PMe_3. Here we report the EDA-NOCV results for $[(PMe_3)_2(E_2H_4)]$ (**1E**), $[(PMe_3)_2(E_2H_2)]$ (**2E**) and $[(PMe_3)_2(E_2)]$ (**3E**).

METHODS

Geometry optimizations have been carried out using TurboMole 6.1 optimizer[10] and gradients at the BP86[11]/def2-TZVPP[12] level of theory. Stationary points were characterized as minima by calculating the Hessian matrix analytically at this level of theory. For all calculations the resolution-of-identity method has been applied.[13]

For the bonding analyses we optimized the molecules with the program package ADF2009.01.[14] BP86 was chosen applying uncontracted Slater-type orbitals (STOs) as basis functions.[15] The latter basis sets for all elements have triple-ζ quality augmented by two sets of polarization functions (ADF-basis set TZ2P). This level of theory is denoted BP86/TZ2P. An auxiliary set of s, p, d, f, and g STOs was used to fit the molecular densities and to represent the Coulomb and exchange potentials accurately in each SCF cycle.[16] Scalar relativistic effects have been incorporated by applying the zeroth-order regular approximation (ZORA) in all ADF calculations.[17]

The interatomic interactions were investigated by means of an energy decomposition analysis (EDA, also known as Extended Transition State method - ETS) developed independently by Morokuma[18] and by Ziegler and Rauk.[19] The bonding analysis focuses on the instantaneous interaction energy ΔE_{int} of a bond A–B between two fragments A and B in the particular electronic reference state and in the frozen geometry of AB. This interaction energy is divided into three main components [Equation (1)].

$$\Delta E_{int} = \Delta E_{elstat} + \Delta E_{Pauli} + \Delta E_{orb} \quad (1)$$

The term ΔE_{elstat} corresponds to the quasiclassical electrostatic interaction between the unperturbed charge distributions of the prepared atoms and is usually attractive. The Pauli repulsion ΔE_{Pauli} is the energy change associated with the transformation from the superposition of the unperturbed electron densities $\rho_A + \rho_B$ of the isolated fragments to the wavefunction $\Psi^\circ = N\,\hat{A}[\Psi_A\Psi_B]$, which properly obeys the Pauli principle through explicit antisymmetrization ($\hat{A}$ operator) and renormalization (N = constant) of the product wavefunction. ΔE_{Pauli} comprises the destabilizing interactions between electrons of the same spin on either fragment. The orbital interaction ΔE_{orb} accounts for charge transfer and polarization effects. The ΔE_{orb} term can be decomposed into contributions from each irreducible representation of the point group of the interacting system. Further details on the EDA/ETS method[14] and its application to the analysis of the chemical bond[20] can be found in the literature.

The EDA-NOCV[21] method combines charge (NOCV) and energy (EDA) decomposition schemes to decompose the deformation density which is associated with the bond formation, $\Delta\rho$, into different components of the chemical bond. The EDA-NOCV calculations provide pair wise energy contributions for each pair of interacting orbitals to the total bond energy. NOCV (Natural Orbital for Chemical Valence)[22,23] is defined as the eigenvector of the valence operator, $\hat{V}$, given by Equation (2):

$$\hat{V}\Psi_i = v_i\Psi_i \quad (2)$$

In the EDA-NOCV scheme the orbital interaction term, ΔE_{orb}, is given by Equation (3):

$$\Delta E_{orb} = \sum_k \Delta E_k^{orb} = \sum_{k=1}^{N/2} v_k \left[-F_{-k,-k}^{TS} + F_{k,k}^{TS} \right] \quad (3)$$

in which $F_{-k,-k}^{TS}$ and $F_{k,k}^{TS}$ are diagonal transitionstate Kohn-Sham matrix elements corresponding to NOCVs with the eigenvalues $-v_k$ and v_k, respectively. The ΔE_k^{orb} term of a particular type of bond are assigned by visual inspection of the shape of the deformation density, $\Delta\rho_k$. The EDA-NOCV scheme thus

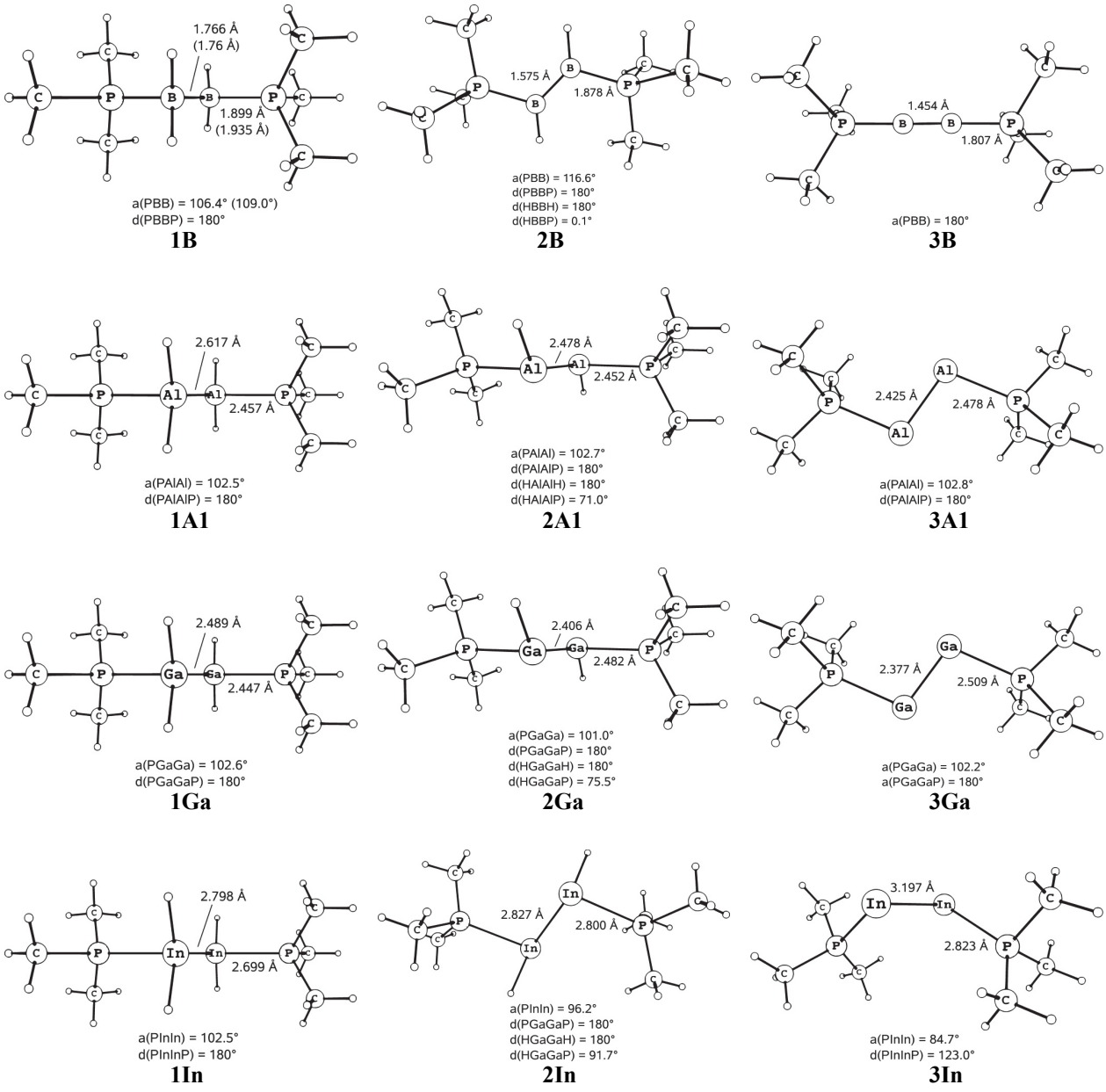

Figure 1. Optimized geometries at RI-BP86/def2-TZVPP and most important bond lengths [Å] and angles [°] of $[(PMe_3)_2(E_2H_n)]$ (E = B − In; n = 4, 2, 0). Experimental values of substituted analogues are given in parentheses.

provides both qualitative ($\Delta\rho_{orb}$) and quantitative (ΔE_{orb}) information about the strength of orbital interactions in chemical bonds, even in molecules with C_1 symmetry.[24]

Wiberg bond indices (WBI), partial charges and Lewis structures were obtained using NBO 3.1[25] as implementted in Gaussian 09 Rev. C.01.[26] NBO electron densities were generated from a single-point calculation of the molecules with BP86/def2-TZVPP basis sets in Gaussian09 from the TURBOMOLE 6.1 optimized geometries.

RESULTS AND DISCUSSION

The optimized geometries of the phosphine complexes **1E**, **2E** and **3E** at def2-TZVPP are shown in Figure 1. The geometrical features have been discussed in our previous studies[1,2] and therefore, we directly proceed to the bonding analysis.

A pivotal question of the EDA-NOCV calculations of complexes $[(L)_2(E_2H_n)]$ is the choice of the electronic states of the interacting fragments for the analysis of the E−E bonds. The present calculations

Table 1. EDA-NOCV results of the E–E bond of $[(PMe_3)_2(E_2H_n)]$ at BP86/TZ2P+. Fragments are $[(PMe_3)(EH_{n/2})$ in doublet (D), triplet (T) or quartet (Q) electronic states. All energies in kcal mol^{-1}

	1E	**2E**	**3E**
E = B	**D**	**T**	**Q**
ΔE_{int}	−86.1	−131.3	−166.7
ΔE_{Pauli}	142.6	166.1	127.5
ΔE_{elstat}	−113.9 (49.8 %)	−142.2 (47.8 %)	−117.1 (39.8 %)
ΔE_{orb}	−114.9 (50.2 %)	−155.2 (52.2 %)	−177.2 (60.2 %)
ΔE_1	−104.3 (90.8 %)	−107.7 (69.4 %)	−98.8 (55.8 %)
ΔE_2		−37.9 (24.4 %)	−35.7 (20.1 %)
ΔE_3			−35.7 (20.1 %)
ΔE_{rest}	−10.6 (9.2 %)	−9.6 (6.2 %)	−7.0 (4.0 %)
E = Al	**D**	**T**	**Q**
ΔE_{int}	−57.5	−82.7	−121.1
ΔE_{Pauli}	72.3	85.9	98.9
ΔE_{elstat}	−75.3 (58.0 %)	−90.4 (53.6 %)	−106.2 (48.3 %)
ΔE_{orb}	−54.6 (42.0 %)	−78.2 (46.4 %)	−113.7 (51.7 %)
ΔE_1	−51.9 (95.1 %)	−47.5 (60.7 %)	−81.3 (71.5 %)
ΔE_2		−28.1 (35.9 %)	−14.5 (12.8 %)
ΔE_3			−15.5 (13.5 %)
ΔE_{rest}	−2.7 (4.9 %)	−2.6 (3.3 %)	−2.4 (2.1 %)

	1E	**2E**	**3E**
E = Ga	**D**	**T**	**Q**
ΔE_{int}	−61.3	−97.8	−149.8
ΔE_{Pauli}	118.4	138.0	163.9
ΔE_{elstat}	−113.3 (63.1 %)	−131.2 (55.6 %)	−149.4 (47.6 %)
ΔE_{orb}	−66.4 (36.9 %)	−104.6 (44.4 %)	−164.2 (52.4 %)
ΔE_1	−61.9 (93.2 %)	−74.7 (71.4 %)	−126.4 (77.0 %)
ΔE_2		−25.2 (24.1 %)	−18.9 (11.5 %)
ΔE_3			−13.5 (8.2%)
ΔE_{rest}	−4.5 (6.8 %)	−4.7 (4.5 %)	−5.4 (3.3 %)
E = In	**D**	**T**	**D**
ΔE_{int}	−54.2	−97.1	−23.6
ΔE_{Pauli}	106.7	111.1	75.6
ΔE_{elstat}	−108.3 (67.3 %)	−115.3 (55.4 %)	−62.9 (64.4 %)
ΔE_{orb}	−52.7 (32.7 %)	−92.9 (44.6 %)	−36.3 (36.6 %)
ΔE_1	−49.5 (93.9 %)	−76.0 (81.8 %)	−32.1 (88.4 %)
ΔE_2		−14.1 (15.2 %)	−2.0 (5.5 %)
ΔE_3			−1.2 (3.3 %)
ΔE_{rest}	−3.2 (6.1 %)	−2.8 (3.0 %)	−1.0 (2.8 %)

were carried out using doublet (D) states for $(PMe_3)EH_2$, triplet (T) states for $(PMe_3)EH$ and quartet states for most of the fragments $(PMe_3)E$ in the EDA-NOCV calculations of **1E**, **2E** and **3E** respectively. The only exception is $(PMe_3)In$ where the inspection of the geometry and the shape of the highest lying MOs indicate that the $(PMe_3)In{-}In(PMe_3)$ bond is a single bond where the interacting fragments are $(PMe_3)In$ in the electronic doublet state. Generally, the choice of the electronic states was made in the light of our earlier results about the electronic structure of the complexes where we analyzed the donor-acceptor bonds $L \rightarrow E_2(H_n) \leftarrow L$.[1,2] The results of the EDA-NOCV calculations are given in Table 1.

The equivalent energy contributions of the α and β electron densities in the EDA-NOCV calculations of the open shell fragments are summed up to give the orbital energy terms ΔE_1 to ΔE_3. Table 1 shows that the orbital interactions ΔE_{orb} in **1E** come mainly from ΔE_1 while the orbital interactions in **2E** have two (ΔE_1 and ΔE_2) and those in **3E** possess three ($\Delta E_1 - \Delta E_3$) major contributions which come from the interactions of the singly occupied orbitals. The remaining orbital interactions ΔE_{rest} are negligible.

Table 1 shows that the interaction energy ΔE_{int} and thus the strength of the E–E bond in $[(PMe_3)_2(E_2H_n)]$ increases with decreasing number of hydrogen atoms *n* 4 < 2 < 0 (Table 1). The only exception is complex **3In** which possesses a very small interaction energy of ΔE_{int} = −23.6 kcal mol^{-1}. Inspection of the equilibrium geometries of **3E** reveals (Figure 1) that **3In** possesses a gauche conformation of the phosphine ligands while the other homologues have either a linear (**3B**) or a trans-bent (**3Al**−**3Ga**) form. It will be shown below that **3In** has a different electronic reference state of the $(PMe_3)In$ fragments than the $(PMe_3)Al$ and $(PMe_3)Ga$ moieties in **3Al** − **3Ga**.

The trend of the E−E interaction energy for different atoms B−In along the series of **1E**−**3E** is very interesting. The calculated data for ΔE_{int} suggest that the Al−Al bonds are always significantly weaker than the B−B bonds which is expected while the Ga−Ga bonds are predicted to be clearly stronger than the Al−Al bonds for all compounds **1E** − **3E**. The In−In bond in **1In** is weaker (−54.2 kcal mol^{-1}) than the Ga−Ga bond in **1Ga** (−61.3 kcal mol^{-1}) but the ΔE_{int} values suggest that the In−In bond in **2In** (−97.1 kcal mol^{-1}) has nearly the same strength as the Ga−Ga bond in **2Ga**

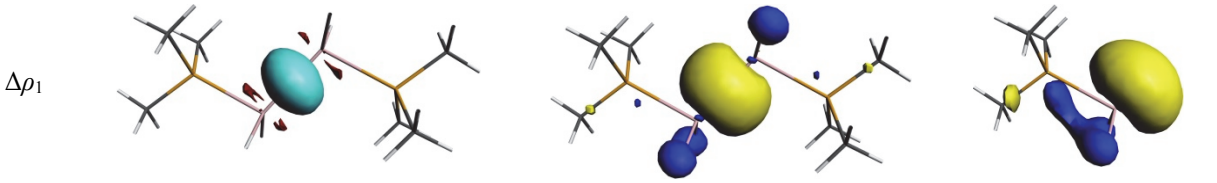

Figure 2. Plot of deformation densities Δρ of the pairwise orbital interactions between two [(PMe$_3$)(AlH$_2$)] fragments in their doublet state, associated energies ΔE in kcal mol^{-1} and eigenvalues ν. Shape of the most important interacting occupied and vacant orbitals of [(PMe$_3$)(AlH$_2$)] and resulting molecular orbitals. $\Delta\rho < 0$ in red, $\Delta\rho > 0$ in light blue.

(−97.8 kcal mol^{-1}). The trend of the E−E bond strengths thus follows the electronegativities of the group-13 atoms B (2.0) > Ga (1.8) > Al (1.5) ~ In (1.5).[27] The In−In bond in **3In** is very weak (−23.6 kcal mol^{-1}). The peculiar trend of the E−E bond strength for different atoms E = B − In shall be elucidated in the light of the EDA-NOCV analysis and NBO calculations.

The EDA-NOCV data for [(PMe$_3$)$_2$(E$_2$H$_4$)] (**1E**) in Table 1 show that the trend of the orbital interaction term ΔE_{orb} has the same order B > Ga > Al > In as the total interaction energy ΔE_{int}. Note that this does not hold for the electrostatic attraction ΔE_{elstat} where the values for **1B** (−113.8 kcal mol^{-1}) and **1Ga** (−113.3 kcal mol^{-1}) are nearly the same and where **1In** (−108.3 kcal mol^{-1}) has a much larger electrostatic attraction than **1A**l (−75.3 kcal mol^{-1}). Very extensive investigations of chemical bonds across the periodic table have shown that the trend of the overall strength of a chemical bond* is in most cases the same as the trend of the orbital interactions.[20] This explains the great success of the model of orbital interactions in chemistry but it must be pointed out that there are exceptions where Pauli repulsion ΔE_{Pauli} or electrostatic interactions ΔE_{elstat} determine the trend of the bond strength.[28]

Table 1 shows that the orbital interactions in **1E** come mainly from one single pair of orbitals. The contribution of ΔE_1 to ΔE_{orb} is always > 90 %. This comes from the pairing of the singly occupied orbitals in (PMe$_3$)EH$_2$ which yield the HOMO of [(PMe$_3$)$_2$(E$_2$H$_4$)]. The shape of the latter orbitals of **1Al** is shown in Figure 2. The orbitals of the other homologues **1B**, **1Ga** and **1In** look very similar and therefore, they are not shown here. Figure 2 gives also the values of ΔE_1 and the eigenvalues ν_1 for all systems along with the plot of the deformation density $\Delta\rho_1$ which is associated with the orbital interactions ΔE_1 in **1Al**. Note that the colour coding of the deformation density $\Delta\rho_1$ indicates the charge flow which has the direction red → blue. The shape of $\Delta\rho_1$ nicely illustrates the charge accumulation in the bonding region of the E−E bond. The EDA-NOCV results suggest a single E−E σ bond for all molecules **1E** which comes from the sharing of the unpaired electrons of the (PMe$_3$)EH$_2$ fragments. This view is supported by the calculated Wiberg bond orders P(E−E) which are shown in Table 2. The calculations give rather uniform values between 0.93 (**1B**) − 0.89 (**1In**). Note that the hybridization of the E−E bonding orbital is nearly constant for the different atoms E. The values are 30.4 % for B, 30.3 % for Al, 31.2 % s for Ga and 30.2 % s for In. This is remarkable, because sp-hybridization of first octal-row atoms is usually much stronger than for heavier atoms due to the different radii of the ns and np valence AOs.[29] The calculated charge distribution shows (Table 2) that the charge donation Me$_3$P → (E$_2$H$_4$) ← PMe$_3$ for the boron compounds is very strong ($\Delta q = -1.42$ *e*) and that the boron atoms carry all of the negative partial charges while the hydrogen atoms have a small positive charge. This means that there is an umpolung of the B−H bonds with respect to normal boranes and that the hydrogen atoms at boron become slightly acidic. The charge donation in the heavier homologues Me$_3$P → E$_2$(H$_4$) ← PMe$_3$ (E = Al − In) has smaller and rather uniform values between −0.64 (Al) and −0.72 (Ga) where the negative charge resides exclusively on the hydrogen atoms while the group-13 atoms carry positive partial charges.

The EDA-NOCV data for [(Me$_3$P)$_2$(E$_2$H$_2$)] (**2E**) in Table 1 show that the strength of ΔE_{orb} has the same order B > Ga > In > Al as the total interaction energy ΔE_{int} but the ΔE_{int} values for the Ga−Ga and In−In bonds are not very different from each other. The orbital interactions in **2E** have two large contributions ΔE_1 and ΔE_2 where the first one is always much larger than the latter. The orbitals of the interacting species of the boron hydride (PMe$_3$)BH yielding **2B** look very different from the MOs of the heavier homologues (PMe$_3$)EH (E = Al − In; Figure 3). This is not surprising, because the equilibrium geometry of **2B** substantially deviates

* Note that the strength of a chemical bond is often not related to the bond dissociation energy (BDE), because the BDE values include also the relaxation of the fragments.

Table 2. NBO results of the E–E bonds at BP86/def2-TZVPP. Partial charges q, bond orders P, occupation and hybridization of the E−E bond orbitals

	$q(E_2H_n)$	q(E)	q(H)	P(E−E)	orbital	Occ.	% s(E)	% p(E)
1B	−1.42	−0.77	0.03	0.93	B−B	1.89	30.4	69.5
1Al	−0.64	0.33	−0.32	0.91	Al−Al	1.89	30.3	69.4
1Ga	−0.72	0.11	−0.23	0.92	Ga−Ga	1.89	31.2	68.7
1In	−0.67	0.19	−0.26	0.89	In−In	1.88	30.2	69.8
2B	−1.26	−0.63	0.00	1.70	B−B	1.94	42.5	57.5
					B−B	1.72	0.0	99.8
2Al	−0.52	0.09	−0.34	1.58	Al−Al	1.86	39.2	60.3
					Al−Al	1.77	11.7	88.0
2Ga	−0.58	−0.02	−0.27	1.49	Ga−Ga	1.82	38.5	61.4
					Ga−Ga	1.76	15.6	84.3
2In	−0.47	0.12	−0.36	1.16	In−In	1.68	36.0	63.9
					In−In	1.68	22.5	77.5
3B	−1.10	−0.55	−	2.41	B−B	1.98	59.3	40.7
					B−B	1.71	0.0	100.0
					B−B	1.71	0.0	100.0
3Al	−0.36	−0.18	−	2.09	Al−Al	1.76	50.7	48.9
					Al−Al	1.75	29.9	70.0
					Al−Al	1.75	0.0	99.8
3Ga	−0.43	−0.22	−	1.94	Ga−Ga	1.69	49.5	50.4
					Ga−Ga	1.70	32.9	67.0
					Ga−Ga	1.77	0.0	99.9
3In	−0.17	−0.09	−	0.85	In−In	1.77	4.3	95.6
					In	1.95	94.5	5.4

from the structures of **2Al** − **2In** (Figure 1). The latter structures have pyramidally coordinated atoms E while **2B** possesses planar coordinated boron atoms.

Figures 3(a) and 3(b) show the shape and eigenvalues of the relevant orbitals of $(PMe_3)BH$ and **2B** and the plot of the deformation densities $\Delta\rho_1$ and $\Delta\rho_2$ along with the associated values of $\Delta E_{1/2}$ and the eigenvalues $v_{1/2}$. The largest contribution ΔE_1 comes from the formation of the B−B σ bond while ΔE_2 comes from the π bond. Note that the associated eigenvalues have the opposite order $v_1 < v_2$, which means that the formation of the weaker π bond involves a larger charge flow than the formation of the σ bond. This can be explained with the shape of the SOMO of LBH where the lobe of the non-bonded part of the orbital is already pointing into the direction of the expected B−B σ bond which requires less distortion for the bond formation than for the π bond.

Figures 3(c) and 3(d) exhibit the shape and eigenvalues of the relevant orbitals of $(PMe_3)AlH$ and **2Al** as well as the associated deformation densities. The shapes of the orbitals and deformations densities of the heavier homologues **2Ga** and **2In** are very similar to those of the aluminum compound and therefore, they are not shown here. The numerical results of the EDA-NOCV calculations are somewhat surprising. The calculated values for ΔE_1 and ΔE_2 suggest that the formation of the σ-type bond which is associated with ΔE_2 (Figure 4d) provides less stabilization energy than the second bond, which can be considered as "slipped" π bond which is the HOMO of the molecules (Figure 3c). The shape of the deformation densities indicates that $\Delta\rho_1$ is associated with a significant reshaping of the π-type lone pair orbitals at $(PMe_3)AlH$ yielding the "slipped" π bond in **2Al** while $\Delta\rho_2$ is associated with the smaller charge accumulation in the σ-bonding region which agrees with the eigenvalues $v_{1/2}$. The large stabilization which is associated with the formation of the HOMO in **2E** (E = Al – In) can be explained with the change in the hybridization of the orbital at atom E which is a pure p AO in $(PMe_3)EH$ but it has between 39.2 % (Al) – 36.0 % (In) s-character in the "slipped" π bond. Table 2 gives the NBO results for the E−E bonds which indicate the polarization and the hybridization of the bonds. The calculated Wiberg bond orders suggest a significant double-bond character for **2Al** (1.58) and **2Ga** (1.49) but less so for **2In** (1.16). In contrast, the EDA-NOCV calculations suggest that the orbital interactions in **2Al** (−78.2 kcal mol^{-1}) are clearly weaker than in **2Ga** (−104.6 kcal mol^{-1}) and **2In** (−92.9 kcal mol^{-1}). Bond orders are related to the numbers of bonding orbitals, but they do not provide information about the strength of the associated stabilization energy. We want to point out that the pyramidal coordination at atom E in **2A**l − **2In** makes it impossible to clearly distinguish between σ and π bonds, because there is no mirror plane in the molecule. The calculated charge distribution shows that the donation $Me_3P \rightarrow E_2(H_2) \leftarrow PMe_3$ for the boron

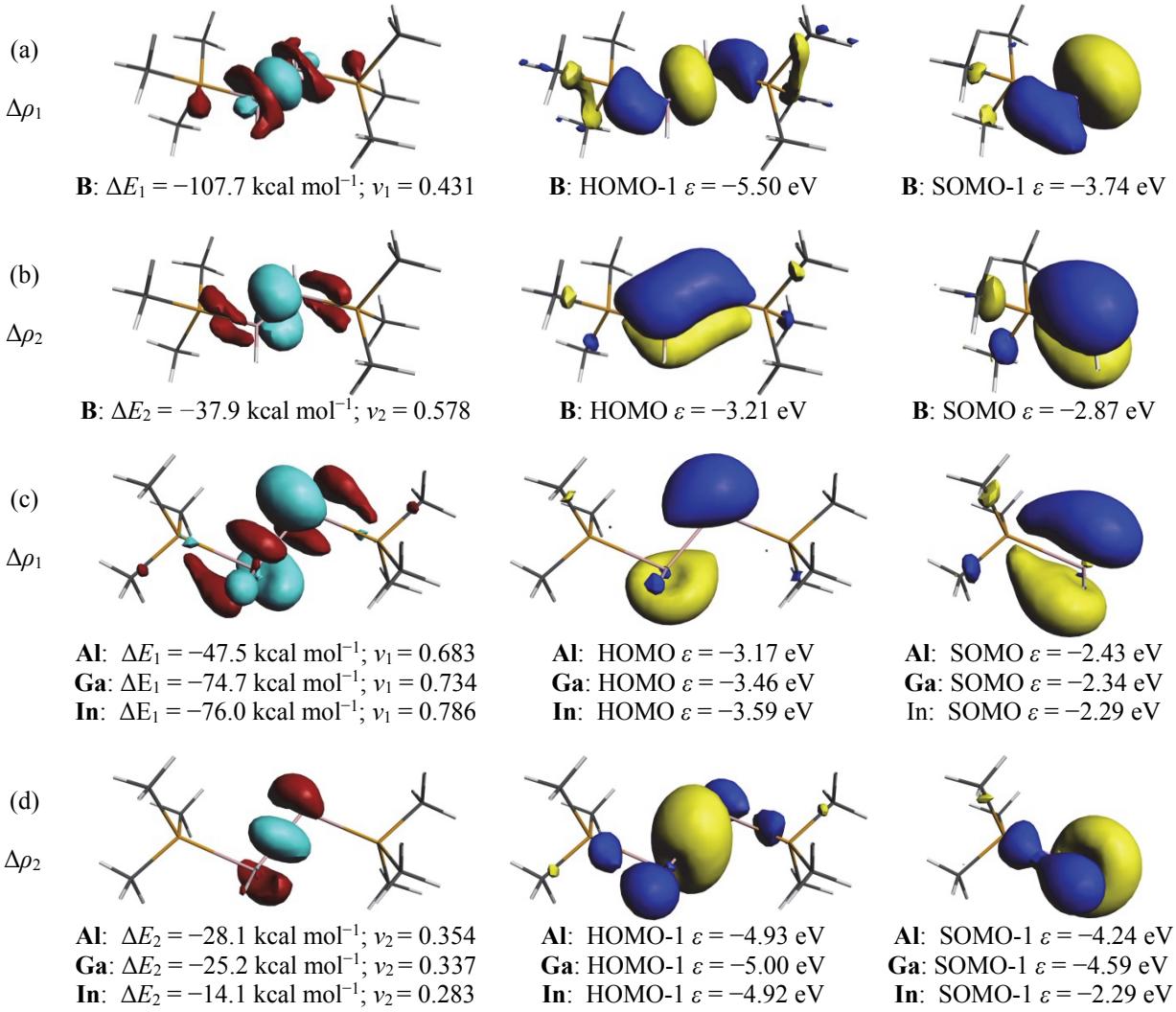

Figure 3. Plot of deformation densities Δρ of the pair wise orbital interactions between (a) and (b) two [(PMe₃)(BH)] fragments and (c) and (d) two [(PMe₃)(AlH)] fragments in their triplet states, associated energies Δ*E* in kcal mol^{-1} and eigenvalues *v*. Shape of the most important interacting occupied and vacant orbitals of [(PMe₃)(EH)] and resulting molecular orbitals. The deformation densities have the direction red → blue.

compounds is rather strong (Δq = −1.26 *e*) and that the boron atoms carry all of the negative partial charges while the hydrogen atoms are neutral. The charge donation in the heavier homologues **2Al** – **2In** is weaker than in **2B** and the negative charge is mainly on the hydrogen atoms. For all systems holds that the charge donation $Me_3P \rightarrow E_2(H_n) \leftarrow PMe_3$ is stronger for n = 4 than for n = 2.

The bonding analysis of the complexes $[(PMe_3)_2(E_2)]$ (**3E**) shall be divided into three parts, because the nature of the interacting orbitals is different for different atoms E. This becomes obvious from the inspection of the equilibrium geometries of **3E** (Figure 1). The linear arrangement $(PMe_3)B{-}B(PMe_3)$ which is also found in the NHC homologue $(NHC^{Dipp})B{\equiv}B(NHC^{Dipp})$ that was recently isolated[7] suggests that the interacting fragment $(PMe_3)B$ has a quartet spin state as reference electronic state. Figure 4 shows the shape and eigenvalues of the relevant orbitals of the boron species **3B** and $(PMe_3)B$ as well as the associated deformation densities. The figures make it clear that $\Delta\rho_1$ refers to the formation of the B−B σ bond while $\Delta\rho_2$ and $\Delta\rho_3$ are associated with the formation of the degenerate B−B π bond. Note that the larger stabilization of the σ bond (−98.8 kcal mol^{-1}) requires less charge flow (v_1 = 0.370) than the π bond which provides a stabilization of −35.7 kcal mol^{-1} for each component with a larger charge deformation ($v_{2/3}$ = 0.583). Table 1 shows that the B≡B triple bond has the strongest interaction energy ΔE_{int} = −166.7 kcal mol^{-1} and also the biggest orbital interaction energy of ΔE_{orb} = −177.2 kcal mol^{-1} of all compounds. According to the

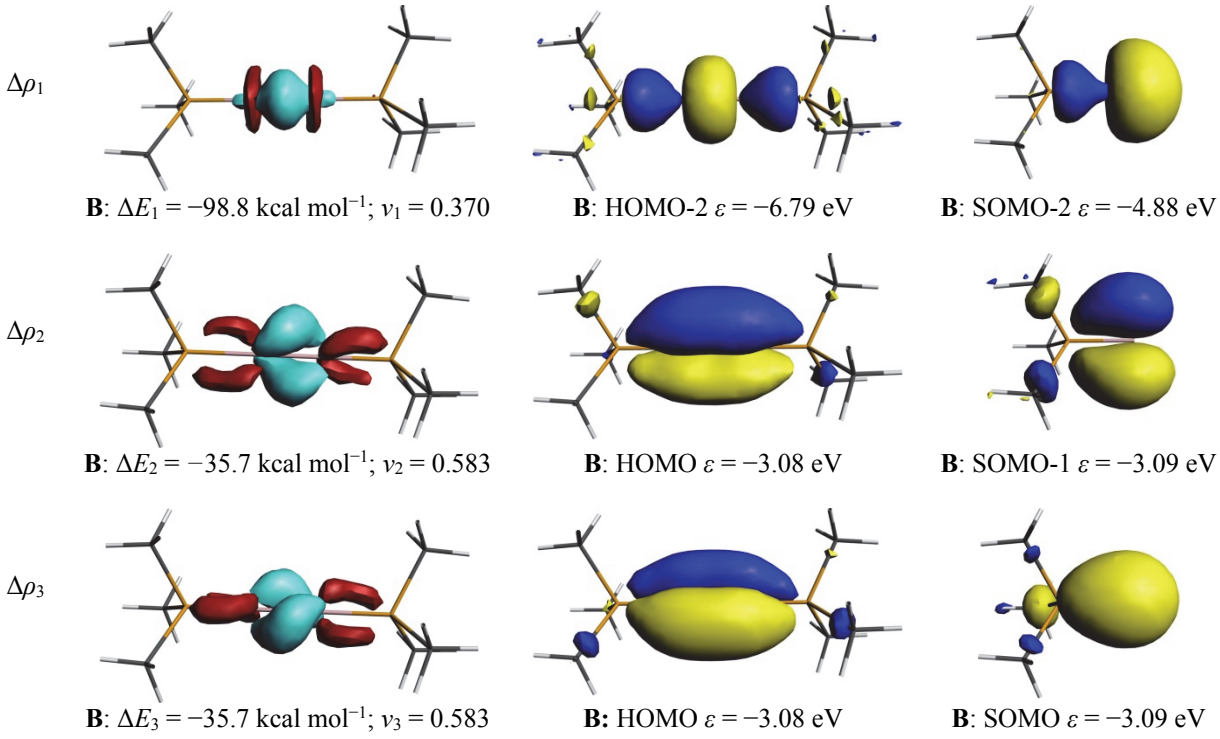

Figure 4. Plot of deformation densities Δρ of the pairwise orbital interactions between two [(PMe_3)(B)] fragments in their quartet state, associated energies ΔE in kcal mol^{-1} and eigenvalues ν. Shape of the most important interacting occupied and vacant orbitals of [(PMe_3)(B)] and resulting molecular orbitals. The deformation densities have the direction red → blue.

EDA-NOCV analysis, the B−B σ bond provides 55.8 % of the covalent bonding while the B−B π bond provides 40.2 % of ΔE_{orb}. The remaining 4.0 % come from lower lying orbitals.

The EDA-NOCV results for the aluminum and gallium analogues **3Al** and **3Ga** are very similar to each other and therefore, we show in Figure 5 only the shape and eigenvalues of the relevant orbitals of **3Al** and (PMe_3)Al with the associated deformation densities, together with the associated numerical values for both compounds. The planar trans-arrangement of the phosphine ligands and the **E2** moieties in **3Al** and **3Ga** (Figure 1) suggest that the electronic reference state of the fragments (PMe_3)Al and (PMe_3)Ga is a quartet state. Table 1 shows that the total interaction energies ΔE_{int} and the orbital interaction energies ΔE_{orb} of **3Al** and **3Ga** using the quartet state of (PMe_3)Al and (PMe_3)Ga are still rather large. The largest contribution to ΔE_{orb} comes from the formation of the "slipped" π bond HOMO-1 which is associated with the charge deformation $\Delta\rho_1$. In contrast, the formation of the σ and π bond (HOMO-2 and HOMO in **3Al** and **3Ga**) stabilizes the molecules much less than the HOMO-1.

Table 1 shows that the In−In bond in **3In** is the weakest E−E bond of all investigated species. It is significantly weaker than the In−In bonds in **1In** and **2In** which deviates from the trend of the other group-13 compounds which have the order **1E** < **2E** < **3E** for the strength of the E−E bond. This can be explained with the electronic state of the fragment (PMe_3)In which is a doublet rather than a quartet. There is thus only one unpaired electron at the fragments which can only form a single bond. Table 1 shows that the stabilizing orbital interactions ΔE_{orb} in **3In** have indeed only one major component ΔE_1 while the lighter homologues have three important components. The dominant orbital interaction is displayed in Figure 6 which shows the shape and eigenvalues of the relevant orbitals of **3In** and (PMe_3)In with the associated deformation density. A comparison of Figure 6 with the results for the aluminum analogue which are shown in Figure 5 reveals interesting differences. The unpaired electron in (PMe_3)In resides in a p(π) AO at In which upon pairing gives the In−In σ bond (Figure 6). In contrast the unpaired p(π) electron in (PMe_3)Al gives upon pairing the "slipped" π bond (Figure 5) whereas the Al−Al σ bond comes mainly from the sp(σ) AO at Al. Note, however, that the doubly occupied MOs in **3Al** and **3Ga** come from a mixture of the MOs of the fragments (PMe_3)E where the SOMOs which are displayed give only the major component.

The NBO results for compounds **3E** (Table 2) show also distinctively different result for **3B**, **3Al**/**Ga** and **3In**. The bond order for the B−B bond in **3B** is 2.41

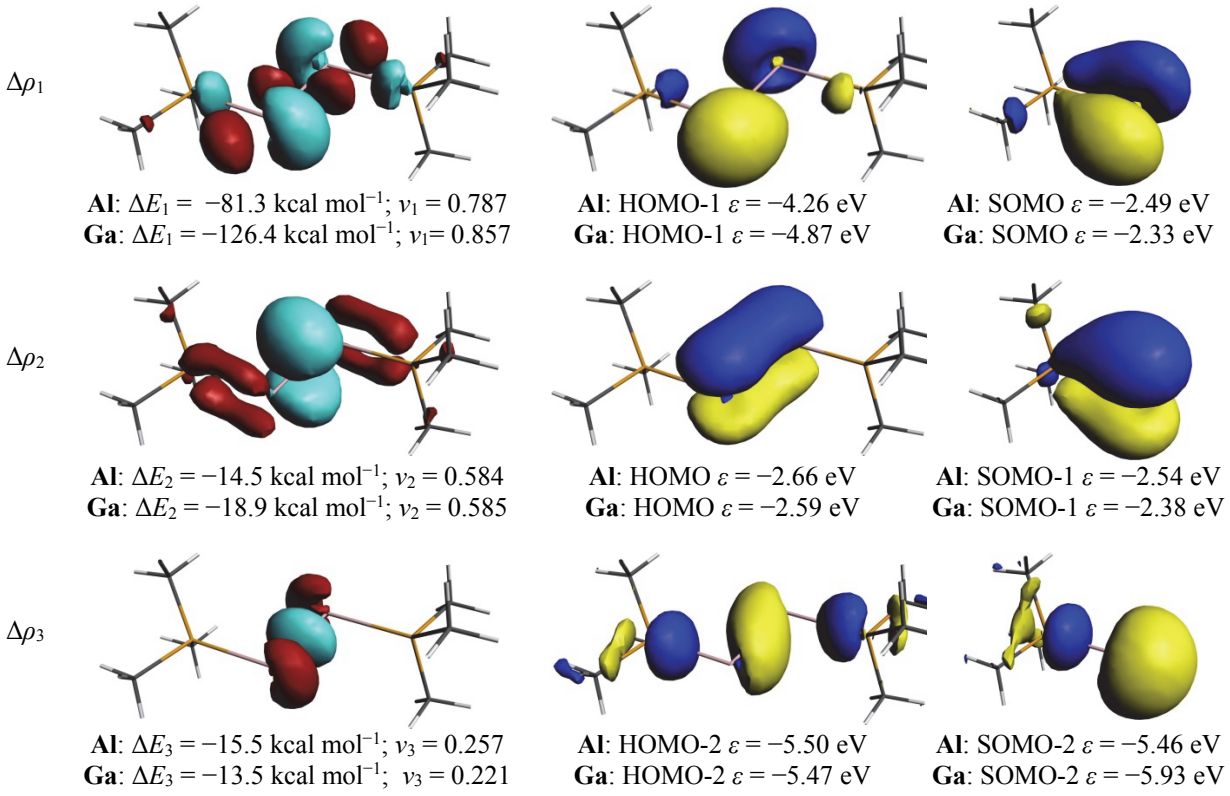

Figure 5. Plot of deformation densities $\Delta\rho$ of the pairwise orbital interactions between two [(PMe$_3$)(Al)] fragments in their quartet state, associated energies ΔE in kcal mol^{-1} and eigenvalues v. Shape of the most important interacting occupied and vacant orbitals of [(PMe$_3$)(Al)] and resulting molecular orbitals. The deformation densities have the direction red → blue.

which supports the assignment of a triple bond. The values of P(E−E) = 2.09 and 1.94 for **3Al**/**Ga** is compatible with a double bond that is supported by a "slipped" π bond, while the value of of P(In−In) = 0.85 for **3In** indicates a single bond. The NBO analysis identifies three E−E bond orbitals for **3B**, **3Al** and **3Ga** but only one In−In bond orbital for **3In** which is mainly composed of p AOs of indium with very little s character. The calculated charge donation $Me_3P \rightarrow E_2 \leftarrow PMe_3$ which is smaller than in **1E** and **2E** has the order B >> Ga > Al > In.

SUMMARY AND CONCLUSION

The results of this work can be summarized as follows. The EDA-NOCV analysis of the E−E interactions in [(PMe$_3$)$_2$(E$_2$H$_n$)] (n = 4, 2, 0) provide deep insights into the nature and the strength of the bonds. The calculated intrinsic interactions ΔE_{int} suggest that the trend for the bond strength of the E−E single bond [(PMe$_3$)(H)$_2$E−E(H)$_2$(PMe$_3$)] has the order B > Ga > Al > In. The orbital interactions ΔE_{orb} which exhibit the same trend as ΔE_{int} have one dominant contribution which comes from

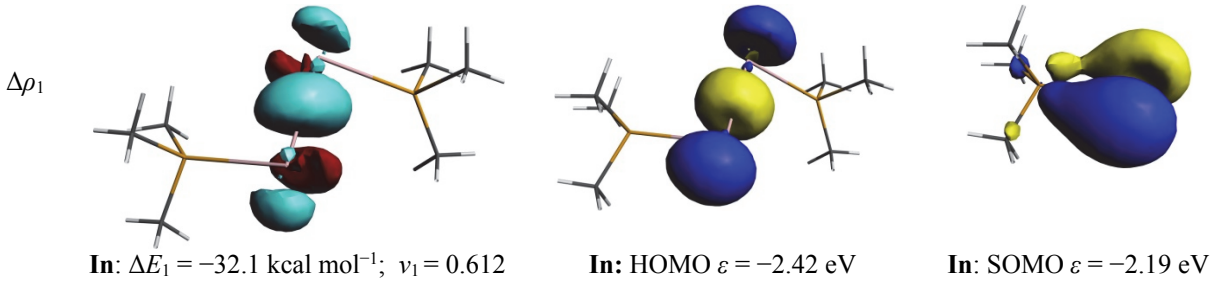

Figure 6. Plot of deformation densities $\Delta\rho$ of the pairwise orbital interactions between two [(PMe$_3$)(In)] fragments in their doublet state, associated energies ΔE in kcal mol^{-1} and eigenvalues v. Shape of the most important interacting occupied and vacant orbitals of [(PMe$_3$)(In)] and resulting molecular orbitals. The deformation densities have the direction red → blue.

the coupling of the singly occupied orbitals in the $(PMe_3)(H)_2E$ fragments. A slightly different trend B > Ga ~ In > Al is found for the interaction energy ΔE_{int} of the E–E bonds in $[(PMe_3)(H)E{-}E(H)(PMe_3)]$. The orbital term ΔE_{orb} which has the order B > Ga > In > Al has one major and one minor component which in case of the boron compound may be identified with a σ and a π bond. The heavier homologues **2E** (E = Al –In) have pyramidally coordinated atoms E. The dominant orbital interactions in the latter species come from the formation of a "slipped" π bond while the minor component comes from the formation of the σ bond. This can be explained with the change in the hybridization of the orbitals at atom E along the formation of the E−E bond. The compounds $[(PMe_3)E{-}E(PMe_3)]$ exhibit three different types of bonding situations depending on atoms E. The boron system **3B** has a classical triple bond which consists of a σ bond that provides 56 % to the orbital interactions and two degenerate π bonds which contribute 40 % to the covalent bonding. The aluminium and gallium complexes **3Al** and **3Ga** are also triply bonded species where the covalent bonding has one strong and two weaker components. The strong component comes from the "slipped" π bond while the minor components come from the formation of the σ and π bonds. The indium complex **3In** has only an In−In single bond and two electron lone pairs at the indium atoms. The charge donation $Me_3P \rightarrow E_2(H_n) \leftarrow PMe_3$ has for all atoms E the trend for n 4 > 2 > 0.

REFERENCES

1. N. Holzmann, A. Stasch, C. Jones, and G. Frenking, *Chem. Eur. J.* **17** (2011) 13517−13525.
2. N. Holzmann, A. Stasch, C. Jones, and G. Frenking, *Chem. Eur. J.* **20** (2013) 6467−6479.
3. Y. Wang, B. Quillian, P. Wei, C. S. Wannere, Y. Xie, R. B. King, H. F. Schaefer III., P. v. R. Schleyer, and G. H. Robinson, *J. Am. Chem. Soc.* **129** (2007) 12412−12413.
4. S. J. Bonyhady, D. Collis, G. Frenking, N. Holzmann, C. Jones, and A. Stasch, *Nature Chem*. **2** (2012) 865−869.
5. Y. Wang, B. Quillian, P. Wei, Y. Xie, C. S. Wannere, R. B. King, H. F. Schaefer III., P. v. R. Schleyer, and G. H. Robinson, *J. Am. Chem. Soc.* **130** (2008) 3298−3299.
6. W. Vandoorne, A. W. Cordes, and G. W. Hunt, *Inorg, Chem.* **12** (1973) 1686−1689.
7. H. Braunschweig, R. D. Dewhurst, K. Hammond, J. Mies, K. Radacki, and A. Vargas, *Science* **336** (2012) 1420−1422.
8. G. Frenking and N. Holzmann, *Science* **336** (2012) 1394−1395.
9. M. P. Mitoraj, A. Michalak, and T. Ziegler, *J. Phys. Chem. A* **112** (2008) 1933−1939.
10. R. Ahlrichs, M. Baer, M Haeser, H. Horn, and C. Koelmel, *Chem. Phys. Lett.* **162** (1989) 165−169.
11. (a) A. D. Becke, *Phys. Rev. A* **38** (1988) 3098−3100; (b) J. P.Perdew, *Phys. Rev. B* **33** (1986) 8822−8824.
12. F. Weigend and R. Ahlrichs, *Phys. Chem. Chem. Phys*. **7** (2005) 3297−3305.
13. K. Eichhorn, O. Treutler, H. Ohm, M. Häser, and R. Ahlrichs, *Chem. Phys. Lett*. **242** (1995) 652−660.
14. (a) F. M. Bickelhaupt and E. J. Baerends, *Rev. Comput. Chem*. **15** (2000) 1−86; (b) G. Te Velde, F. M. Bickelhaupt, E. J. Baerends, C. Fonseca Guerra, J. A. Van Gisbergen, J. Snijders, and T. Ziegler, *J. Comp. Chem*. **22** (2001) 931−967.
15. J. G. Snijders, E. J. Baerends, and P. Vernoojs, *At. Data Nucl. Data Tables* **26** (1981) 483−509.
16. J. Krijn and E. J. Baerends, *Fit Functions in the HFS-Method; Internal Report* (in Dutch), Vrije Universiteit Amsterdam, The Netherlands (1984).
17. E. Van Lenthe, E. J. Baerends, and J. G. Snijders, *J. Chem. Phys*. **99** (1993) 4597−4610.
18. K. Morokuma, *J. Chem. Phys*. **55** (1971) 1236−1244.
19. T. Ziegler and A. Rauk, *Inorg. Chem.* **18** (1979) 1755−1759.
20. (a) G. Frenking, K. Wichmann, N. Fröhlich, C. Loschen, M. Lein, J. Frunzke, and M. Rayón, *Coord. Chem. Rev.* **238−239** (2003) 55−91; (b) M. Lein and G. Frenking, *Theory and Applications of Computational Chemistry: The First 40 Years*, p. 367−414, Elsevier, Amsterdam (2005); (c) A. Krapp, F. M. Bickelhaupt, and G. Frenking, *Chem. Eur. J.* **12** (2006) 9196−9216; (d) G. Frenking and F. M. Bickelhaupt, *The Chemical Bond. 1. Fundamental Aspects of Chemical Bonding*, p. 121−158, Wiley-VCH, Weinheim, 2014.
21. M. P. Mitoraj, A. Michalak, and T. Ziegler, *J. Chem. Theory Comput.* **5** (2009) 962−975.
22. M. P. Mitoraj and A. Michalak, *Organometallics* **26** (2007) 6576−6580.
23. M. P. Mitoraj and A. Michalak, *J. Mol. Model.* **14** (2008) 681−687.
24. (a) D. Devarajan and G. Frenking, *Chem. Asian J.* **7** (2012). 1296−1311; (b) T. A. N. Nguyen and G. Frenking, *Chem. Eur. J.* **18** (2012) 12733−12748; (c) N. Holzmann, D. Dange, C. Jones, and G. Frenking, *Angew. Chem*. **125** (2013) 30783083; (d) M. Mousavi and G. Frenking, *Organometallics* **32** (2013) 1743−1755; (e) A. Das, C. Dash, M. A. Celik, M. Yousufuddin, G. Frenking, and H. V. R. Dias, *Organometallics* **32** (2013) 3135−3144; (f) M. A. Celik, G. Frenking, B. Neumüller, and W. Petz, *ChemPlusChem*. **78** (2013) 1024−1032; (g) T. A. N. Nguyen and G. Frenking, *Mol. Phys*. **111** (2013) 2640−2646; (h) M. Hermann, C. Goedecke, C. Jones, and G. Frenking, *Organometallics* **32** (2013) 6666−6673.
25. A. E. Reed, R. B. Weinstock, and F. Weinhold, *J. Chem. Phys.* **83** (1985) 735−746.
26. M. J. Frisch et al., *Gaussian09, Rev. C.01,* Gaussian Inc., Wallingford CT, (2009).
27. A. L. Allred and E. G. Rochow, *J. Inorg. Nucl. Chem*. **5** (1958), 264−290.
28. (a) G. Frenking, K. Wichmann, N. Fröhlich, J. Grobe, W. Golla, D. Le Van, B. Krebs, and M. Läge, *Organometallics* **21** (2002) 2921−2930; (b) C. Esterhuysen and G. Frenking, *Theoret. Chem. Acc*. **111** (2004) 381−390.
29. (a) W. Kutzelnigg, *Angew. Chem*. **96** (1984) 262−288; (b) P. Pyykkö, *J. Chem. Res*. (S) (1979) 380−381.